HNNC Radical and Its Role in the CH + N_2 Reaction†

Michael R. Berman

Air Force Office of Scientific Research, 875 North Randolph Street, Arlington, Virginia 22203

Takashi Tsuchiya, Adriana Gregušová, S. Ajith Perera,* and Rodney J. Bartlett

Quantum Theory Project, Department of Chemistry and Physics, University of Florida, Gainesville, Florida 32611

Received: March 25, 2007; In Final Form: May 10, 2007

A previously unreported channel in the spin-allowed reaction path for the CH + N_2 reaction that involves the HNNC radical is presented. The structures and energetics of the HNNC radical and its isomers HCNN and HNCN and the relevant intermediates and transition states that are involved in the proposed mechanism are obtained at the coupled cluster singles and doubles level of theory with noniterative triples correction (CCSD(T)) using a converging series of basis sets aug-cc-pVDZ, aug-cc-pVTZ, and aug-cc-pVQZ. The aug-cc-pVQZ basis is used for all the final single point energy calculations using the CCSD(T)/aug-cc-pVTZ optimized geometries. We find the HNNC radical to have a heat of formation of $\Delta_f H_0$ (HNNC) = 116.5 kcal mol^{-1}. An assessment of the quality of computed data of the radical species HNCN and HCNN is presented by comparison with the available experimental data. We find that HNNC can convert to HNCN, the highest barrier in this path being 14.5 kcal mol^{-1} above the energy of the CH + N_2 reactants. Thus, HNNC can play a role in the high-temperature spin-allowed mechanism for the reaction of CH + N_2 proposed by Moskaleva, Xia, and Lin (*Chem. Phys. Lett.* **2000**, *331*, *269*).

I. Introduction

The reaction of CH with N_2 is of considerable importance at low temperatures in the chemistry of planetary atmospheres and at high temperatures in combustion chemistry. The low-temperature reaction proceeds by the barrierless formation of a datively bonded addition complex, HCNN.[1−4] At the high temperatures of combustion environments, the reaction is believed to be dominated by pathways that lead to the production of the "prompt" NO seen in flames.[5] Initially, a spin-forbidden pathway in which HCN ($X^1\Sigma^+$) + N(^{4}S) are produced had been postulated,[6−14] whereas more recently, Lin and co-workers[15] proposed that the dominant route in combustion produces H + NCN ($^3\Sigma^-_g$) in a spin-allowed process that passes through an HNCN intermediate. Further theoretical and experimental studies have supported the spin-allowed pathway.[16−18]

The multiple pathways available in the CH + N_2 reaction highlight the richness of detail in the potential energy surface for this system. There are numerous intermediates that possibly can be formed, several of which can be stabilized as stable molecules. For example, both HCNN and HNCN have been produced from other processes and studied in photoelectron experiments[18−21] and they have been studied theoretically as well.[22] On the other hand, the HNNC isomer of these molecules is not well-known. In the CH + N_2 system, the HNNC intermediate can directly dissociate to H + CNN products, which are considerably higher in energy than H + NCN. More importantly, the HNNC intermediate can connect other structures on the potential energy surface and can open previously unconsidered pathways that must be included to fully map out the potential energy surface in this system.

In this paper, high-level electronic structure calculations are performed on the CH + N_2 system with particular emphasis on the HNNC intermediate and the pathways on the potential energy surface that involve this intermediate. Because accurate energies and vibrational frequencies of transition states and intermediates are essential to performing reliable kinetic analyses, calculations are performed using the CCSD(T) method with correlation consistent basis sets. To establish that the basis set limit is reached, structures, frequencies, and energies of the species on the CH + N_2 potential energy surface (PES) that are relevant to the current work were computed using aug-cc-pVDZ and aug-cc-pVTZ basis sets for all the structures, and with the aug-cc-pVQZ basis set for selected structures that have been identified as critical. The CCSD(T) method is often regarded as the method of choice to treat electron correlation and its performance has been exhaustively calibrated against experiment.[23,24]

II. Computational Methods

The geometry optimizations and vibrational frequencies are computed at the CCSD(T)[25] level with Dunning et al. augmented correlation consistent polarized valence basis sets aug-cc-pVDZ and aug-cc-pVTZ.[26,27] The CCSD(T) Hessians are calculated numerically differentiating analytically computed gradients. In addition, CCSD(T)/aug-cc-pVQZ single-point energies are performed at the CCSD(T)/aug-cc-pVTZ geometry. Spherical harmonic atomic orbital basis functions are used and all the electrons are correlated. The relative energies are presented with reference to the sum of CH and N_2 ground state energies calculated at the corresponding computational level. All the energies are corrected for zero point vibrations [zero-point-energy correction (ZPE)] using the vibrational frequencies of normal modes computed at the same level except for those at

† Part of the special issue "M. C. Lin Festschrift".

10.1021/jp0723618 CCC: $37.00
Published on Web 07/03/2007

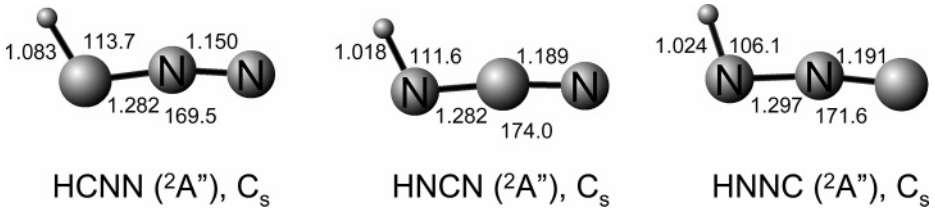

Figure 1. Equilibrium structures of HCNN, HNCN, and HNNC optimized at the CCSD(T)/aug-cc-pVTZ level. Bond lengths are given in angstroms, and angles are in degrees. The symmetries of the molecules and their electronic states (in parentheses) are also shown.

TABLE 1: Bond Lengths (in Å), Bond Angles (in Degrees), Vibrational Frequencies (in cm^{-1}), Atomization Energies (in kcal mol^{-1}), Relative Energies with Respect to CH + N_2 (in kcal mol^{-1}), and Heats of Formation (in kcal mol^{-1}) for HCNN, HNCN, and HNNC, Calculated at the CCSD(T)/aug-cc-pVQZ Level for the CCSD(T)/aug-cc-pVTZ Geometries[a]

	HCNN	HNCN	HNNC
r([C]N−N); *r*([N]C−N); *r*([N]N−C)	1.150	1.189	1.191
r(H−C); *r*(H−N); *r*(H−N)	1.083	1.018	1.024
r([H]C−N); *r*([H]N−C); *r*([H]N−N)	1.282	1.282	1.297
a(CNN); *a*(NCN); *a*(NNC)	169.5	174.0	171.6
a(HCN); *a*(HNC); *a*(HNN)	113.7	111.6	106.1
atomization energy	331.9	367.2	327.4
relative energy	−29.6	−65.0	−25.1
heat of formation, $\Delta_f H_0$	112.0	76.7	116.5
Harmonic vibrational frequencies	538, 541, 912, 1219, 1897, 3183	408, 479, 1081, 1172, 1901, 3498	318, 333, 1064, 1374, 2000, 3402

[a] Energies are corrected with ZPE obtained at CCSD(T)/aug-cc-pVTZ level.

the CCSD(T)/aug-cc-pVQZ level. In the case of CCSD(T)/aug-cc-pVQZ energies, the ZPEs computed at the CCSD(T)/aug-cc-pVTZ level are used. To verify that the CCSD(T)/aug-cc-pVTZ level geometries were converged with respect to basis set for all practical purposes, selected sets of structures based on their importance (reactants, products, and the HCNN linear complex), are optimized at the CCSD(T)/aug-cc-pVQZ level as well. Intrinsic reaction coordinate (IRC) calculations are performed at the CCSD/6-31G** level[28,29] to ensure that the reactants and products of the reactions are connected via the relevant transition states for each of the reactions under consideration. The transition states are reoptimized and the vibrational frequencies of normal mode are recalculated at that level, and the IRC searches followed along the direction parallel to the normal mode corresponding to the imaginary frequencies. The ACES II program system[30] is used for all the calculations.

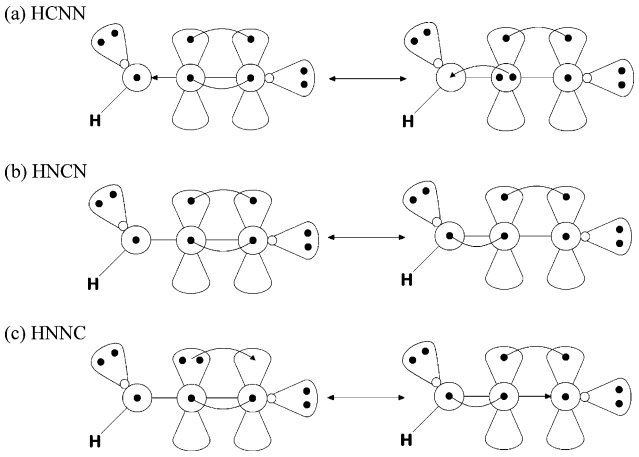

Figure 2. Schematic representation of the resonance structures of the ground states of (a) HCNN, (b) HNCN, and (c) HNNC.

III. Results and Discussion

A. HNNC Radical. The structures and vibrational and photoelectron spectra of HCNN and HNCN have been the subject of several previous experimental[18−21] and theoretical[22] investigations because they have been identified as playing a critical role in the CH + N_2 reaction. However, our present work led us to consider the HNNC radical, which can also play a role in the aforementioned reaction. A full theoretical characterization of HNNC and a comparison of its structure, bonding, and energetics with its known isomers at the CCSD-(T)/aug-cc-pVTZ level is presented.

The CCSD(T)/aug-cc-pVTZ structure of the HNNC radical is shown in Figure 1 along with the analogous structures of the isomers HCNN and HNCN. In Table 1 we report the relative energies, atomization energies, heats of formation, and the harmonic vibrational frequencies as well as the geometries (also shown in Figure 1) of the three radicals.

All the radicals have been calculated to have planar structures (C_s symmetry), and their ground electronic states are $^2A''$. According to the CCSD(T)/aug-cc-pVTZ calculations, the triple and double bond lengths of N−N (C−N) bonds are 1.100 Å (1.169 Å) and 1.213 Å (1.353 Å), respectively. The tabulated standard N−N and (C−N) triple, double, and single bond distances are 1.10 Å (1.16 Å), 1.25 Å (1.32 Å), and 1.45 Å (1.47 Å), respectively.[31] The terminal N−N, C−N, and N−C bond lengths of HCNN, HNCN, and HNNC are 1.150, 1.189, and 1.191 Å, respectively, all of which are closer to the corresponding triple bond distances. On the other hand, the lengths of C−N, N−C, and N−N bonds next to the terminal bond (1.282, 1.282, and 1.297 Å, respectively) are closer to the double bond distances. This can be formally described by resonance mechanisms as shown in Figure 2.

The ground states of all three radicals can be represented with two resonance structures. By averaging the contributions of both structures, it can be seen that the bond order of the terminal N−N or C−N bonds are formally 2.5, whereas that of the bonds next to the terminal bonds are formally 1.5, which shows a reasonable agreement with our calculated bond lengths. The electron population analysis provides strong support to this resonance mechanism. The electron populations of each atom in HCNN are formally, 1.0, 7.0, 6.0, and 7.0 for H, C, N, and

TABLE 2: Experimental and Theoretical Values for Bond Lengths (in Å), Bond Angles (in Degrees), Vibrational Frequencies (in cm^{-1}), and Electron Affinities (in kcal mol^{-1}) for the Ground ($^2A''$) State of (a) HNCN and (b) HCNN[a]

(a) HNCN

	r(NCN)	*r*(NH)	*a*(CNH)	N−C−N stretch	N−C−N out of plane bending	electron affinity
exptl	2.47 ± 0.002[b]	1.034 ± 0.002[b]	116.5 ± 2.7[b]	1140[c]	440[c]	−38.9 ± 0.14[d]
this work	2.471	1.018	111.6	1172	479	−39.2

(b) HCNN

	H−CNN stretch	HC−N−N asym stretch	H−CNN bend	electron affinity
exptl	3233 (Ar matrix)[e]	1787 (Ar matrix)[e]	861 (Ar matrix)[e]	−60.5 ± 0.12[f]
	3229 (N_2 matrix)[e]	1784 (Kr matrix)[e]	860 (Kr matrix)[e]	
		1800 (N_2 matrix)[e]	871 (N_2 matrix)[e]	
this work	3183	1897	912	−60.4

[a] The theoretical values were calculated at the CCSD(T)/aug-cc-pVTZ level [b] Reference 33. [c] Reference 34. [d] Reference 19. [e] References 35 and 36. [f] Reference 20.

N (in the order of bonding), respectively. The Mulliken population analysis for the calculated ground state HCNN shows the electron populations of H, C, N, and N to be 0.55, 6.46, 6.20, and 7.42, respectively, which well reproduce the formal values. It can be seen that the H and C atoms have lower electron populations than their formal values whereas two N atoms have more than what are formally expected. The detailed analysis reveals that the σ-orbitals are more delocalized over the entire molecule, which makes bonding tighter. In fact, the C−N bond length (1.282 Å) is shorter than the double bond distance (1.353 Å), which shows the bond order is more than 2, and the formal bond order is 1.5. The calculated spin populations (electron population difference between α- and β-orbitals) of the π-orbitals (a'') on C and terminal N are 0.53 and 0.46, respectively. This agrees very well with the resonance mechanism: the unpaired electron is localized on C in one structure, and it is localized on the terminal N in the other structure. The C−N−N angle (169.5°) is distorted from the linear value. This can be explained from the resonance structures to be attributed to the electron repulsion between the lone-pair in one of the sp^2-hybridized orbital on C and the electrons in the π-bonding orbital, both of which are in the symmetry plane. The calculated (formal) atomic electron populations in HNCN are 0.67 (1.0), 7.10 (7.0), 5.72 (6.0), and 7.14 (7.0) for H, N, C, and N, respectively. Again, transfer of an electron from H and C to N atoms can be observed, which makes the N−C bond lengths (1.282 Å) shorter than the double bond distance (1.353 Å). The spin population of the a'' π-orbitals on N and N (terminal) are 0.58 and 0.47, respectively, which, again, agrees well with the resonance mechanism. The same analysis can be applied to HNNC. The calculated (formal) electron populations on H, N, N, and C are 0.68 (1.0), 7.26 (7.0), 6.36 (6.0), and 6.35 (7.0), respectively. The electron transfer from C to N occurs also in this radical. However, an interesting difference is observed regarding the bond length in this radical. The N−N bond length has been calculated to be 1.297 Å and is significantly longer than the double bond distance (1.213 Å) whereas the lengths of the corresponding bonds of the other radicals (1.282 Å for C−N bond in HCNN and 1.282 Å for N−C bond in HNCN) are both shorter than the double bond distance (1.353 Å). The spin population of the a'' π-orbitals on N (next to H) and C have been calculated to be 0.72 and 0.25, respectively. The remarkably large spin population (0.72) on N shows that the resonance structure with an unpaired electron localized on N is dominant. The N−N bond is formally single in the dominant resonance structure, but it is formally double in the other resonance structure. This explains why the N−N bond length is noticeably longer in HNNC compared to the lengths of the corresponding bond (C−N in HCNN and N−C in HNCN) relative to the corresponding double bond distances.

The relative energies of HNCN (−65.0 kcal mol^{-1}), HCNN (−29.6 kcal mol^{-1}), and HNNC (−25.1 kcal mol^{-1}) radicals with respect to CH + N_2 shown in Table 1 indicate (together with the atomization energies and heats of formation) that the stability of the three radicals are in the order of HNCN > HCNN > HNNC where HNCN is the most stable. This stability can be described by considering the bond energies in part. For brevity, we assume that all the C−N and N−N are doubly bonded. Note that the average formal bond orders are 2.5 for the terminal bond and 1.5 for the next bond, respectively; thus it is a good approximation to assume both of them to be double bonds for qualitative discussion. The standard bond energy of the C−N double bond is 147 kcal mol^{-1} whereas that of the N−N double bond is 100 kcal mol^{-1}.[32] It is easily understood that HNCN is the most stable isomer among the three because HNCN has two C−N bonds and the other two isomers have one C−N bond and one N−N bond each. However, in this context, it is expected that HCNN and HNNC have the same relative energies, or it can rather be expected that HNNC is more stable than the HCNN because the C−N bond length is shorter in HNNC (1.191 Å) compared to that in HCNN (1.282 Å). However, our calculation predicted HCNN to be more stable than HNNC by 4.5 kcal mol^{-1}. This may be attributed to resonance. In HCNN, two resonance structures contribute equally whereas, in HNNC, one structure is dominant.

Both HNCN and HCNN have been detected in photoelectron experiments of their negative ions.[18−21] Both radicals are short-lived (20 ± 5 ns) and only a limited set of experimental structure and spectroscopic data are available in the literature for HNCN, and shown in Table 2, along with the computed CCSD(T)/aug-cc-pVTZ results. Very little is known about the HCNN molecule. The electron affinity observed in matrix isolation experiments of H_2CN_2 by mercury lamp irradiation and the observed IR active fundamental frequencies are shown in Table 2 along with the corresponding computed values. We have not been able to find any reference to the HNNC radical in the literature.

Although there are numerous theoretical studies of the HNCN and HCNN using a plethora of theoretical methods, a comparison of current results with prior theoretical work is not within the context of this paper, and they will be the subject of a comprehensive follow up paper on the CH + N_2 reaction. Nevertheless, it is worthwhile to mention that the present calculations which employ the CCSD(T) method with aug-cc-

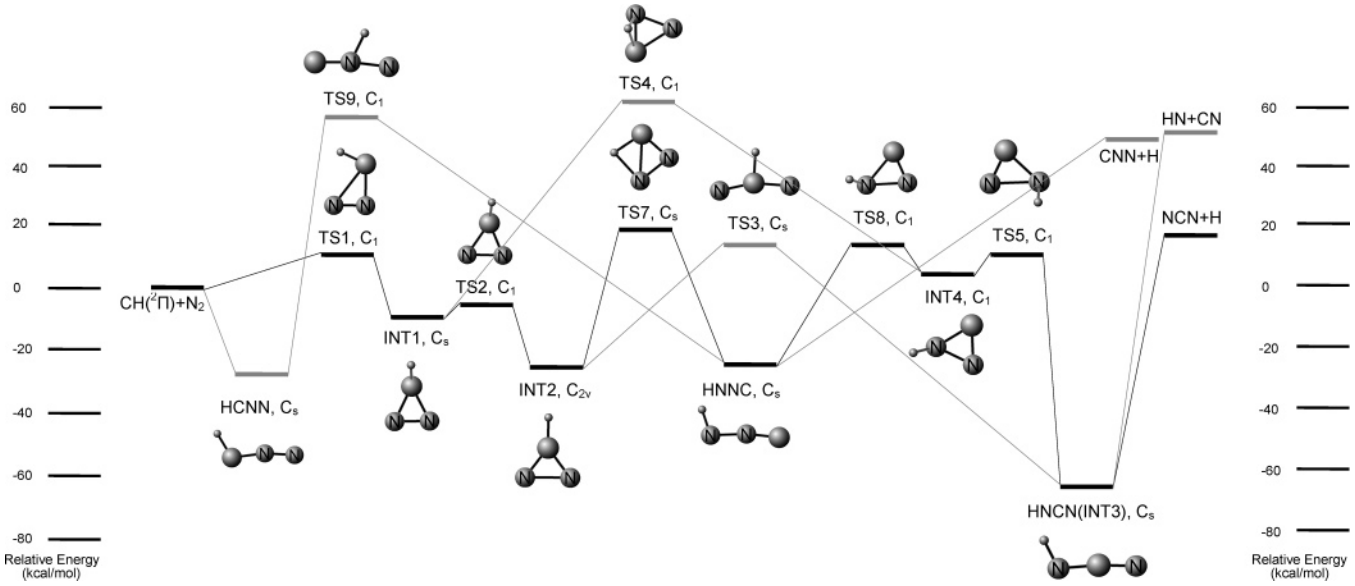

Figure 3. Schematic representation of the spin-allowed reaction mechanism. The energies are calculated at the CCSD(T)/aug-cc-pVQZ level; geometries and ZPE are calculated at the CCSD(T)/aug-cc-pVTZ level. The names of intermediates and transition states are consistent with those used by Moskaleva et al.[15] for the same structures.

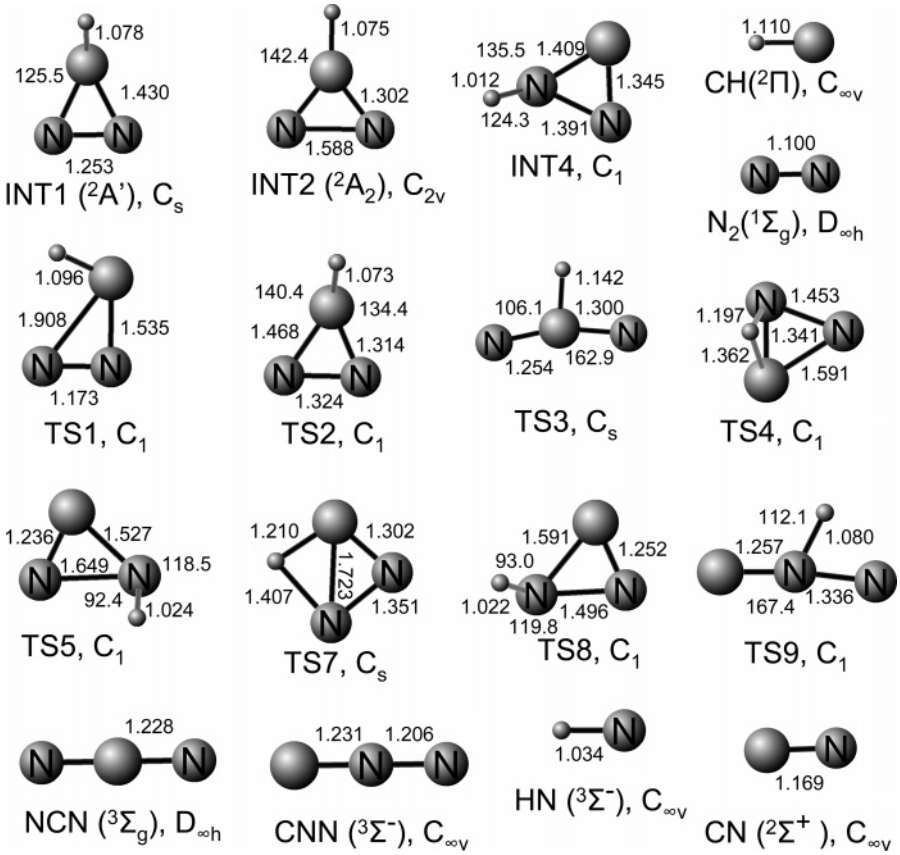

Figure 4. CCSD(T)/aug-cc-pVTZ structures of the reactants, products, intermediates, and transition states involving in the reaction shown in Figure 3. Bond lengths are given in angstroms, and angles are in degrees. The symmetries of the molecules and their electronic states (in parenthesis) are also shown. See Figure 1 for HCNN, HNCN, and HNNC.

pVTZ (aug-cc-pVQZ for single point energy calculations) are the most definitive calculations to date, and should have the capability of being "predictive" for the CH + N_2 system.

B. Reaction Mechanisms. The first study of the CH + N_2 system that incorporated the H + NCN reaction channel was performed by Moskaleva et al.[15] The names of intermediates and transition states used here are consistent with those used by Moskaleva et al. for the same structures. A portion of the potential energy diagram for the CH($^2\Pi$) + N_2 reaction that involves the HNNC intermediate is shown in Figure 3. Detailed structures of the species shown in the potential energy diagram are shown in Figure 4, and the energies of the species relative to the energy of CH + N_2 reactants are listed in Table 3 along with energies calculated by Moskaleva et al.[15] Generally, there is good agreement, within 2−3 kcal mol^{-1}, found between their results using the G2M method and the CCSD(T) results

TABLE 3: Energies Relative to the Reactants (ZPE Corrected; in kcal mol^{-1}) of the Reactants, Products, Intermediates, and Transition States Involved in the Reaction Shown in Figure 3[a]

	energy	
	this work	G2M(RCC2)[b]
CH($^2\Pi$) + N_2	0.0	0.0
TS1	9.9	12.2[c]
INT1	−8.8	−9.8[c]
TS2	−5.0	−4.8[d]
INT2	−24.6	−23.5[d]
TS7	20.0	
HNNC	−25.1	
TS8	14.5	
TS4	59.4	45.7[c]
INT4	5.9	4.5[c]
TS5	11.6	15.8[c]
TS3	14.4	11.7[d]
HNCN (INT3)	−65.0	−61.1[c]
H + NCN ($^3\Sigma^-_g$)	17.8	21.5[d]
H + CNN ($^3\Sigma^-$)	47.4	
TS9[e]	54.0	
HCNN	−29.6	−27.8[d]
HN + CN	49.5	

[a] The energies are calculated at the CCSD(T)/aug-cc-pVQZ level; geometries and ZPE are calculated at the CCSD(T)/aug-cc-pVTZ Level. The G2M(RCC2) energies reported by Moskaleva et al.[15] are also shown. [b] See ref 15 and references therein. [c] Geometries are optimized with B3LYP/6-311G(d,p) method. [d] Geometries are optimized with MP2/6-311G(d,p) method. [e] TS9 is planar (C_s symmetry) at both CCSD/6-31G** and CCSD/6-311G** levels and IRC confirms that it connects both to HCNN and to HNCC. However, at the CCSD(T)/aug-cc-pVTZ level it distorts to a nonplanar structure (7° distortion of the H−N bonding from the C−N−N plane) and the frequency analysis shows that there is still a 16i cm^{-1} imaginary frequency corresponding to the angle bend in addition to the 1948i cm^{-1} imaginary frequency corresponding to the reaction coordinate. Perhaps further refinement of the structure will eliminate the second small imaginary frequency; however, we find that the nature of the transition state region prevents further automatic refinement of the transition state structure.

presented here, the largest differences being for transition states TS4 and TS5, where differences are 13.7 and 4.2 kcal mol^{-1}, respectively.

In the reaction mechanism, we find that CH can insert across the N−N triple bond through a transition state TS1 with a barrier of 9.9 kcal mol^{-1} and then exothermically rearrange into cyclic intermediates of C_s symmetry (INT1) and C_{2v} symmetry (INT2). The barrier height for the initial insertion is slightly lower than but consistent with the value of 10.8 kcal mol^{-1} reported by Moskaleva et al.[15] The barrier going from INT1 to INT2 through transition state TS2 is 3.8 kcal mol^{-1}, again in good agreement with that found by Moskaleva et al.[15] The lowest energy spin-allowed pathway from INT2 to INT3 (which can dissociate to NCN + H products) goes through transition state TS3, which we find to be a little higher in energy than Moskaleva et al. with an energy of 14.4 kcal mol^{-1} above CH + N_2 at the CCSD-(T)/aug-cc-pVTZ level compared to 11.7 kcal mol^{-1} at the G2M(RCC) level in ref 15. Takayanagi[17] finds a barrier of 31.1 kcal mol^{-1} from INT2 to TS3 calculated at the CASPT2(11_e,-11_o)/cc-pVTZ level (not ZPE corrected) compared to 35.2 kcal mol^{-1} for Moskaleva et al.[15] and our ZPE-corrected value of 39.0 kcal mol^{-1}. TS3, which has a ring structure of C_s symmetry in which the C-atom has inserted between the two N atoms, can undergo an exothermic ring opening and hydrogen shift to form INT3 (HNCN).

Moskaleva et al. reported another pathway to HNCN in which INT1 proceeded over a much higher energy barrier (TS4), which could then proceed exothermically through several intermediates to INT3 (HNCN). We find that the energy of TS4 computed at the CCSD(T)/aug-cc-pVQZ using CCSD(T)/aug-cc-pVTZ optimized geometry is 59.4 kcal mol^{-1} relative to the reactants, which is significantly higher (13.7 kcal mol^{-1}) than the value of 45.7 kcal mol^{-1} reported by Moskaleva et al.[15] Our TS4 structure is slightly different from the one reported in ref 15. In our structure, the hydrogen atom is almost on the C−N bond (see Figure 4) whereas, in Moskaleva et al.,[15] the hydrogen is more outside of the C−N−N ring. Moskaleva et al.[15] report that they were unable to locate TS4 beyond MBPT(2)/6-311G-(d,p) level of theory, and we believe that the differences in structure and energies of TS4 between the two studies are due to more complete treatment of the electron correlation effects in the work reported here.

In this work, we find an additional possible route from INT1 to INT3 (and NCN + H products) through the INT2, HNNC, and INT4 intermediates. The highest barrier in this pathway is at TS7, 20.0 kcal mol^{-1} above reactants at the CCSD(T)/aug-cc-pVQZ level, a barrier considerably lower in energy than the route through TS4, and only 5.6 kcal mol^{-1} higher than the highest energy (TS3) in the pathway from INT2 to INT3. The barrier at TS7 is only 2.2 kcal mol^{-1} higher than the endothermicity for the H + NCN product channel; thus we expect the pathway to HNNC over TS7 to be reasonably accessible under combustion conditions.

We find several possible pathways from the HNNC minimum on the potential energy surface. The lowest energy pathway leads to HNCN (INT3), as mentioned above, by first going through a cyclic transition state, TS8, located 14.5 kcal mol^{-1} above the CH + N_2 reactants, and forming INT4. There is then a barrier of 8.6 kcal mol^{-1} for going from INT4 to TS5 in which the N−N bond has been stretched to 1.649 Å. The ring opening from TS5 to form HNCN is then exothermic by 76.6 kcal mol^{-1}. Because the energy barriers in going from HNNC to HNCN are all smaller than the energy needed to dissociate HNCN to H + NCN, interconversion of HNNC and HNCN by this pathway should be viable under combustion conditions. We note that Moskaleva et al.[15] found INT5 and TS6 between TS5 and HNCN at the MP2 level whereas no intermediate nor transition state was found in our CCSD(T)/aug-cc-pVTZ calculation. We have performed the IRC calculation at the CCSD/6-31G** level and confirmed that TS5 and HNCN are directly connected. A second pathway from the HNNC minimum is the dissociation to H + CNN. The energy of these dissociation products are 47.4 kcal mol^{-1} above CH + N_2 and 29.6 kcal mol^{-1} above H + NCN products. Another pathway from HNNC is the isomerization to HCNN through a migration of the hydrogen atom along the NNC backbone. This process has a large barrier with the transition state TS9 located 83.7 kcal mol^{-1} above HNNC. We also note that the dissociation of HNNC to HN + CN is endothermic by 74.7 kcal mol^{-1}.

IV. Conclusions

The energy and structure of the previously unreported HNNC radical has been predicted and investigated theoretically by means of highly accurate state-of-the-art CCSD(T) calculations. It is shown that the equilibrium structure of HNNC is planar (C_s symmetry) and the ground electronic state is $^2A''$, exhibiting similarity with its well studied isomers, HCNN and HNCN. The ground state electronic configurations can be described formally by considering two resonance structures, as has been done for the other isomers. On the other hand, significant differences are also found between HNNC and its isomers, in both its geometrical and electronic structures. The N−N bond length

in HNNC is longer, unlike the corresponding bonds in the other isomers, which are shorter relative to their corresponding double bond distances. The unpaired electron in the a″ π-orbitals has been found to be considerably localized on the N (next to H) atom in HNNC contrary to that in the other isomers, which are equally distributed on two atoms, as is formally expected from the resonance mechanism. Those observations imply that only one resonance structure is dominant in HNNC whereas the other isomers have equal contribution from two resonance structures. The HNNC radical has been calculated to be slightly less stable (by ca. 4 kcal mol^{-1}) than HCNN, the latter of which has been observed by experiment.[20,36]

The HNNC radical was found to have a role in the high-temperature reaction pathway of CH + N_2. The isomer, HNCN, is believed to play a critical role in this reaction by dissociating into the products NCN + H, which further leads to "prompt NO". It has been shown that the HNNC is accessible from CH + N_2 reactants under combustion conditions and is capable of reaching HNCN through reasonably low barriers on the potential surface. Thus, although the reaction path from the C_{2v} INT2 structure to HNCN is still the lowest energy spin-allowed pathway from reactants to NCN + H products, pathways including HNNC are accessible and should be considered in developing a complete picture of the high-temperature reactions in the CH + N_2 system.

Acknowledgment. This paper honors the scientific contributions of M. C. Lin. His creativity and seminal contributions in experimental and theoretical studies have been an inspiration to us. The University of Florida group (T.T., A.G., S.A.P., and R.J.B.) acknowledge the support of the United States Air Force office of Scientific Research under the grant No. FA 9550-07-1-0070 and a Phase II STTR to ACES Q.C. and the University of Florida, FA 9550-07-C-0033.

References and Notes

(1) Berman, M. R.; Lin, M. C. *J. Phys. Chem.* **1983**, *87*, 3933−3942.
(2) Brownsword, R. A.; Herbert, L. B.; Smith, I. W. M.; Stewart, D. W. A. *J. Chem. Soc., Faraday Trans.* **1996**, *92*, 1087−1094.
(3) Fulle, D.; Hippler, H. *J. Chem. Phys.* **1996**, *105*, 5423−5430.
(4) Le Picard, S. D.; Canosa, A. *Geophys. Res. Lett.* **1998**, *25*, 485−488.
(5) Miller, J. A.; Bowman, C. T. *Prog. Energy. Combust. Sci.* **1989**, *15*, 287−338.
(6) Lindackers, D.; Burmeister, M.; Roth, P. *23rd Symp. (Int.) Combust. Proc.* **1990**, 251−257.
(7) Dean, A. J.; Hanson, R. K.; Bowman, C. T. *23rd Symp. (Int.) Combust. Proc.* **1990**, 259−265.
(8) Becker, K. H.; Engelhardt, B.; Geiger, H.; Kurtenbach, R.; Schrey, G.; Wiesen, P. *Chem. Phys. Lett.* **1992**, *195*, 322−328.
(9) Becker, K. H.; Geiger, H.; Wiesen, P. *Int. J. Chem. Kinet.* **1996**, *28*, 115−123.
(10) Manaa, M. R.; Yarkony, D. R. *J. Chem. Phys.* **1992**, *95*, 1808−1816.
(11) Seideman, T. *J. Chem. Phys.* **1994**, *101*, 3662−3670.
(12) Rodgers, A. S.; Smith, G. P. *Chem. Phys. Lett.* **1996**, *253*, 313−321.
(13) Cui, Q.; Morokuma, K. *Theor. Chem. Acc.* **1999**, *102*, 127−133.
(14) Cui, Q.; Morokuma, K.; Bowman, J. M.; Klippenstein, S. J. *J. Chem. Phys.* **1999**, *110*, 9469−9482.
(15) Moskaleva, L. V.; Xia, W. S.; Lin, M. C. *Chem. Phys. Lett.* **2000**, *331*, 269−277.
(16) Moskaleva, L. V.; Lin, M. C. *Proc. Combust. Inst.* **2000**, *28*, 2393−2401.
(17) Takayanagi, T. *Chem. Phys. Lett.* **2003**, *368*, 393−398.
(18) Bise, R. T.; Hoops, A. A.; Neumark, D. M. *J. Chem Phys.* **2001**, *114*, 9000−9011.
(19) Clifford, E. P.; Wenthold, P. G.; Lineberger, W. C.; Petersson, G. A.; Ellison, G. B. *J. Phys. Chem. A* **1997**, *101*, 4338−4345.
(20) Clifford, E. P.; Wenthold, P. G.; Lineberger, W. C.; Petersson, G. A.; Broadus, K. M.; Kass, S. R.; Kato, S.; DePuy, C. H.; Bierbaum, V. M.; Ellison, G. B. *J. Phys. Chem. A* **1998**, *102*, 7100−7112.
(21) Bise, R. T.; Hoops, A. A.; Choi, H.; Neumark, D. M. *J. Chem. Phys.* **2000**, *113*, 4179−4181.
(22) Puzzarini, C.; Gambi, A. *J. Chem. Phys.* **2005**, *122*, 064316.
(23) Helgaker, T.; Jørgensen, P.; Olsen, J. *Molecular electronic-structure theory*; John Wiley & Sons: Chichester, U.K., 2000.
(24) Bartlett, R. J.; Musial, M. *Rev. Mod. Phys.* **2007**, *79*, 291−352.
(25) Ragavachari, K.; Trucks, G. W.; Pople, J. A.; Head-Gordon, M. *Chem. Phys. Lett.* **1989**, *157*, 479−483.
(26) Dunning, T. H., Jr. *J. Chem. Phys.* **1989**, *90*, 1007−1023.
(27) Kendall, R. A.; Dunning, T. H., Jr.; Harrison, R. J. *J. Chem. Phys.* **1992**, *96*, 6796−6806.
(28) Purvis, G. D., III; Bartlett, R. J. *J. Chem. Phys.* **1982**, *76*, 1910−1918.
(29) Hariharan, P. C.; Pople, J. A. *Theor. Chim. Acta* **1973**, *28*, 213−222.
(30) Stanton, J. F.; Gauss, J.; Watts, J. D.; Nooijen, M.; Oliphant, N.; Perera, S. A.; Szalay, P. G.; Lauderdale, W. J.; Kucharski, S. A.; Gwaltney, S. R.; Beck, S.; Balková, A.; Bernholdt, D. E.; Baeck, K. K.; Rozyczko, P.; Sekino, H.; Hober, C.; Pittner, J.; Bartlett, R. J., 1993; ACES II is a product of the Quantum Theory Project, University of Florida. Integral packages included are VMOL (Almlöf, J.; Taylor, P. R.); VPROPS (Taylor, P.); and a modified version of the ABACUS integral derivative package (Helgaker, T.; Jensen, H. J. Aa.; Jørgensen, P.; Olsen, J.; Taylor, P. R.).
(31) Petrucci, R.H. *General chemistry: principles and modern applications*, 5th ed.; Macmillan Publishing Co.: New York, 1989.
(32) Sanderson, R.T.; *Chemical bonds and bond energy*, 2nd ed.; Academic Press: New York, 1976.
(33) Herzberg, G.; Warsop, P. A. *Can. J. Phys.* **1963**, *41*, 286−298.
(34) Wu, M.; Hall, G.; Sears, T. J. *J. Chem. Soc., Faraday Trans.* **1993**, *89*, 615−621.
(35) Jacox, M. E. *Vibrational and Electronic Energy Levels of Polyatomic Transient Molecules*; American Institute of Physics: Woodbury, NY, 1994; p 11797.
(36) Ogilvie, J. F. *Can. J. Chem.* **1968**, *46*, 2472−2474.